62-2-6

FINAL ENGINEERING REPORT FOR PHASE I OF TUNABLE MASER DEVELOPMENT

REPORT NO. 8431-2

Prepared for

NAVY DEPARTMENT, BUREAU OF SHIPS
ELECTRONICS DIVISION

INDEX NO. SS022001/ST1

Date of Report: 24 November 1961
Period Covered: 1 April 1960 through 30 November 1961

CUTLER-HAMMER

AIRBORNE INSTRUMENTS LABORATORY
DEER PARK, LONG ISLAND, NEW YORK

AIL DIVISION

FINAL ENGINEERING REPORT FOR PHASE I OF TUNABLE MASER DEVELOPMENT

by

F. Arams and B. Peyton

Prepared for

Navy Department, Bureau of Ships
Electronics Division
Index No. SS022001/ST1

REPORT NO. 8431-2

Date of Report: 24 November 1961
Period Covered: 1 April 1960 through 30 November 1961

Airborne Instruments Laboratory
A Division of Cutler-Hammer, Inc.
Deer Park, Long Island, New York

ACKNOWLEDGMENTS

The authors wish to thank F. Kirpal for assistance with the experiments, and S. Okwit, H. Lewis, H. Gerritsen, and D. Carter for various discussions related to the project.

This work was supported, in part, by Aeronautical Systems Division, Wright-Patterson Air Force Base, Ohio.

TABLE OF CONTENTS

		Page
I.	Summary	1
II.	Introduction	3
III.	Maser Material	5
	A. Selection of Material	5
	B. Angular Orientation of Rutile	5
IV.	TWM Structure	9
	A. Mode Considerations	9
	B. Matching Techniques	11
	C. Slowing Factor	12
V.	Experimental Results at Liquid Helium Temperatures	13
	A. Low-Field Operation	13
	B. High-Field Operation	14
	C. Experimental and Calculated Structure Loss	17
	D. Pump Saturation	17
	E. Linewidth	17
VI.	Ferrite Isolation	21
VII.	Final Packaging Considerations	23
	A. Final Maser Packaging Considerations	23
	B. Further Improvements	25
VIII.	Conclusions	27
IX.	References	29
	Appendix--Calculated Performance of Millimeter-Wave Maser Using Push-Pull Pumping in Rutile	31

LIST OF ILLUSTRATIONS

Figure

1 Comparison of Various Push-Pull-Pumped Maser Materials

2 Signal Frequency vs Magnetic Field for Push-Pull-Pumped Chromium-Doped Rutile

3 Pump Frequency vs Magnetic Field for Push-Pull-Pumped Chromium-Doped Rutile

4 Calculated Rutile Tuning Curves

5 Experimental Ridged Waveguide Structure Loaded with Cr^{+3} : TiO_2 Crystal and Two Polycrystalline Matching Pieces

6 Insertion Loss of TWM Structure at Room Temperature

7 Operating Frequencies for Rutile-Loaded Maser Structure

8 Experimental Maser Data

9 Electronic Gain and Inversion Ratio vs Signal Frequency

10 Maser Pump Saturation Curve

11 Reverse Isolator Loss vs Applied Magnetic Field at Room Temperature

12 Folded TWM Structure Having an Active Length of 2.3 Inches

13 Slowing Factor and Insertion Loss vs Frequency for Ridged Slow-Wave Structure

A-1 Normalized Signal Absorption vs Idler Frequency with Bath Temperature as a Parameter

A-2 Normalized Electronic Gain vs Idler Frequency with Bath Temperature as a Parameter

A-3 Calculated Inversion Ratio vs Idler Frequency with Bath Temperature as a Parameter

I. SUMMARY

The design of a millimeter-wave traveling-wave maser (TWM) has been successfully tested. This TWM combines the features of:

1. K_a-band (26 to 40 kMc) operation,
2. Unprecedented tuning range (for example, 33 to 40 kMc),
3. Ultra-low noise (0.2-db noise factor expected)--first low-noise amplifier in this band,
4. Two-port device,
5. Ferrite isolators--developed to ensure gain stability even with severe load mismatches,
6. Tunable by varying magnetic field and pump frequency only,
7. Design suitable for operation in other frequency bands (for example, 18 to 26.5 kMc, or 12.4 to 18 kMc),
8. Shows feasibility of developing practical masers at the present time for operation at signal frequencies of 150 kMc and higher.

A number of maser materials and pumping schemes were investigated, and push-pull-pumped chromium-doped TiO_2 was chosen as the most desirable active material for a maser amplifier operating in K_a-band with wide-range tuning capability. Various transmission lines were investigated. Broadband structures and auxiliary apparatus were designed.

Maser action was successfully obtained in chromium-doped TiO_2 over the entire 26 to 40 kMc band, using very low pump frequencies (43 to 47.5 kMc) and low magnetic fields (0.7 to 6 kilo-oersteds).

Maser action was next obtained at the high magnetic field region (23.5 to 27 kMc and from 33.5 to 39.5 kMc). Elec-

tronic gains averaging 8.8 db per inch were obtained from 23.5 to 27 kMc using pump frequencies from 64 to 72.6 kMc at $4.2^{o}K$ and 14 db per inch in the 33.5 to 39.5 kMc region at $1.7^{o}K$ using a pump frequency from 62 to 76 kMc. It is estimated that a maser amplifier having 25 db of net gain can be constructed for the 33 to 40 kMc band using 2-1/2 inches of active material with optimum chromium concentration.

Isolators of nickel-zinc ferrite were successfully incorporated into the maser structure to ensure stable operation. The ferrite tuning curve overlapped the rutile tuning curve from 33 to 41 kMc at $4.2^{o}K$ and suppressed any oscillations in the structure. The forward loss of the isolators was less than 0.5 db, and the reverse loss was 25 to 50 db.

Rutile crystals of different chromium dopings were tested and the optimum chromium-doping was determined to be 0.065 percent Cr^{+3} by weight.

II. INTRODUCTION

Low-temperature experiments combined with theoretical analysis were carried out to provide data for the selection of (1) the most suitable maser material and pumping techniques, (2) the best angular orientations of the crystal consistent with pump frequency and applied magnetic field requirements, (3) a low-loss traveling-wave structure that is capable of being operated over a large frequency range, and (4) ferrite isolators that will contribute sufficient reverse loss to increase stable operation of the TWM amplifier.

III. MASER MATERIAL

A. SELECTION OF MATERIAL

For millimeter-wave masers, one very important consideration is the strength of the applied magnetic field, as a function of zero-field splitting parameter 2D for four-level maser crystals with axial symmetry (E = 0), where D and E are crystal field parameters. Figure 1 shows magnetic field requirements for push-pull pumping as a function of the zero-field splitting factor for various maser materials with signal frequency as a parameter. In general, it is seen that as low a zero-field splitting as possible is desirable, but this must be weighted against the drop-off in the pump transition probability at magnetic fields where the signal frequency exceeds the zero-field splitting frequency. As Figure 1 shows, in the case of chromium-doped rutile, the presence of the E-term in the Spin Hamiltonian is important in minimizing magnetic field requirements in the high-field region, where high gains can be obtained.

Based on this consideration and those that were discussed in previous reports, we have chosen chromium-doped titanium dioxide as the most suitable maser material for the frequency band of interest.

B. ANGULAR ORIENTATION OF RUTILE

Although certain energy-level diagrams of Cr^{+3} in TiO_2 are available (references 1, 2, and 3), we have carried out our own computations to obtain accurate data on the energy levels in this material for push-pull maser operation. The results are shown in Figure 2 for the signal frequency f_{23} and

in Figure 3 for the pump frequency $f_p = f_{13} = f_{24}$ with the following parameters.

Θ = orientation of H with respect to C-axis,

ϕ = orientation of H with respect to the x-axis, which is the magnetic axis of one of the complexes of Cr^{+3} in TiO_2.

Figure 4 shows, in greater detail, the portions of the rutile tuning curves of Figure 2 that are of interest in tuning the band for 27 to 40 kMc. As can be seen, two crystal orientations, and hence two maser structures each with a different crystal orientation, are required to cover the band, because of magnetic field and pump tuning range limitations. Two alternatives are shown:

	Angle Θ (in degrees)	Tuning Range (in kMc)
A.	60	26.5 to 35
	72.5	33.5 to 40
B.	62.5	26.5 to 33.5
	80	33.5 to 40

For the two alternatives, the maximum magnetic fields are 13.5 and 12.8 kilogauss, respectively. Pump frequency is in the 60 to 90 kMc region where klystrons have become available.

When the crystal is oriented at $\Theta = 54.7^\circ$, $\phi = 45^\circ$ (Figure 2), the two crystal sites are aligned so that their energy levels coincide, and twice the electronic gain is obtained. Using this favorable angle, a single-head maser can be tuned from 27 to 40 kMc when the magnetic fields change from 12 to 17 kilogauss. This large magnet tuning range might be obtained from a superconducting magnet.

Operation in lower-frequency bands, for example, 12.4 to 18 kMc, and 18 to 26.5 kMc, can be obtained for the same pump frequency and magnetic fields by operating at other angular orientations.

Pump frequency is minimized by using push-pull pumping, where the pump frequency can be lower than twice the signal frequency.

IV. TWM STRUCTURE

A. MODE CONSIDERATIONS

The desirable characteristics of a TWM structure include (1) low circuit loss for both signal and pump frequencies, (2) high slowing factor (long electrical length for given physical length), (3) ease of coupling the signal and pump frequencies into the crystal over a large frequency band, (4) high filling factor for pump and signal, (5) well-defined regions of circular polarization, (6) single-mode propagation for the signal over the tuning range, (7) simple geometry for the maser crystal, and (8) minimum size to reduce magnet weight.

Consideration was given at the outset to the following transmission structures.

1. Rectangular waveguide TE_{10} mode,
2. Circular waveguide TE_{01} (low-loss) mode,
3. Rutile waveguide dielectric mode (work of Okaya at Columbia University).

It must be kept in mind that rutile is highly anisotropic, which makes operation over a large frequency band difficult.

Calculations were carried out for the circuit losses to be expected for the various modes. The results are listed in Table I for a rutile waveguide with a cutoff frequency of 20 kMc operating at room temperature.

According to the data of Pippard measured at 1200 Mc, the conductivity of silver improves 3.5 times when cooled from room temperature to $4.2^{\circ}K$. Furthermore, the loss tangent of chromium-doped rutile is as low as 2×10^{-5} at

TABLE I

THEORETICAL CIRCUIT LOSSES OF RUTILE WAVEGUIDE

Waveguide	Mode	Dimensions in inches	Wall Loss (silver) in db/cm	Dielectric Loss (10^{-4} loss tangent) in db/cm	Total Circuit Loss in db/cm
Rectangular	TE_{10}	0.015 x 0.030	0.48	0.03	0.51
Circular	TE_{11}	0.0173 diameter	0.24	0.03	0.27
Circular	TE_{01}	0.0366 diameter	0.06	0.03	0.09

4.2°K. It is concluded that the circuit loss of fully loaded rutile waveguide in the TE_{10} mode is probably as low as 0.30 db/cm at liquid helium temperature, so that this mode offers the best potential because (1) it has planes of circular polarization, (2) ease of matching over large frequency bands, (3) it is a dominant mode, and (4) the moding due to crystal anisotropy can be prevented by decreasing the waveguide height.

B. MATCHING TECHNIQUES

The problem of matching an air-loaded (0.140 × 0.280 inch I.D.) waveguide to a rutile (approximately 0.015 × 0.030 inch I.D.) waveguide, which has a very low impedance because of its dielectric constant (greater than 100), was overcome using tapered sections of undoped polycrystalline TiO_2. The polycrystalline TiO_2 has a dielectric constant near 80 at room temperature. To maintain a good match, it is desirable to keep the cutoff frequency nearly constant in the transition region. This problem has been handled by the use of (1) ridged waveguide (Figure 5) and (2) dielectric-loaded tapered waveguide.

1. RIDGED WAVEGUIDE STRUCTURE

Structures were built using quadruply ridged waveguide transitions for the purpose of matching both the TE_{10} signal-frequency mode as well as the higher-frequency pump mode, which might be launched in the TE_{01} mode. Figure 6 shows insertion loss as a function of signal frequency for a copper ridged structure. As can be seen, the loss is near 4.0 db over the 25 to 40 kMc band at room temperature.

2. TAPERED WAVEGUIDE STRUCTURE

In this matching technique, the waveguide height is first tapered to the height of the rutile waveguide (0.026 to 0.030 inch). This reduces the waveguide impedance by a factor

of about 5. The waveguide width is then tapered while dielectric loading is introduced. The transition can be rigorously designed using K15 or K25 stycast tapers, using the design curves of Vartanian (reference 4).

3. RUTILE WAVEGUIDE

Figure 7 shows the experimental upper and lower frequency limits of our structure as a function of the width of the titania sliver with bath temperature as a parameter.

As can be seen, for a given crystal width the pass band of the structure shifts as the temperature is reduced. This shift is caused by the fact that the dielectric constant of the material increases by about 45 percent as the crystal is cooled from room to helium temperatures, thereby reducing the waveguide cutoff frequencies and impedance by 21 percent.

If, for example, RG-96/U waveguide were used in the input and output of the TWM, a crystal about 0.030 inch wide would keep the lower cutoff frequency constant at 4.2°K and thereby improve the match and maximize the tuning range of the structure. Reduction of the width of the maser crystal so that the waveguide is not fully loaded did not significantly affect the slowing because of the high dielectric constant of rutile.

C. SLOWING FACTOR

A slowing factor, and hence increase in gain, of 9 was measured at room temperature in the structure. This increase is due to dielectric slowing caused by the high dielectric constant (greater than 100) of the rutile.

V. EXPERIMENTAL RESULTS AT LIQUID HELIUM TEMPERATURES

A. LOW-FIELD OPERATION

The initial experiments on maser action in chromium-doped rutile were done in the low-field region to become familiar with the energy levels, the line-up procedure, and experimental techniques.

Population inversion was successfully obtained over the entire range from 23 to 40 kMc using pump frequencies from 47.5 to 43 kMc and magnetic fields from 6 to 0.7 kilo-oersteds (Figure 8). The magnetic field vector was in the AC plane at $\Theta = 54.7^{\circ}$, $\phi = 45^{\circ}$ where the two magnetic complexes of Cr^{+3} in TiO_2 are aligned. The signal and idler frequencies become equal at 24.1 kMc. Near this frequency, maser operation is not possible for $\Theta = 54.7^{\circ}$, and therefore this limits the tuning range to 25 to 40 kMc. The various operating points for the signal and pump frequency are shown as solid points in Figure 8. As can be seen, a very large tuning range is obtained with a pump source operating at relatively low frequency and tuned over a relatively narrow range.

Inversion at 40 kMc, using a pump at a frequency of only 43 kMc, at an applied magnetic field as low as 700 oersteds is especially noteworthy, because of the lack of success in obtaining maser action in push-pull pumped ruby at a similar point in the low-field region (reference 5).

When the temperature was reduced from $4.2^{\circ}K$ to $1.6^{\circ}K$ in the 25 to 30 kMc range, the absorption increased by a factor of 2 and was in agreement with the theoretical value of 2.1.

B. HIGH-FIELD OPERATION

After the initial experiments at low magnetic fields, all subsequent work was done at high fields where higher gains per unit length and alignment with ferrite isolators can be obtained. Magnetic absorption and maser action have so far been observed at four push-pull crystal orientations (Figure 8):

Angle θ (degree)	Signal Frequency (kMc)	Magnetic Field (kilogauss)
54.7	23.0 to 31.0	10.0 to 13.7
66.0	27.5 to 31.0	8.0 to 11.0
80.0	33.0 to 40.0	8.0 to 12.0
90.0	33.5 to 37.5	7.5 to 10.5

Our early work was concentrated on the $\theta = 54.7^{\circ}$, $\phi = 45^{\circ}$ orientation because of (1) the ease of alignment due to its inherent symmetry and (2) the repeatability of the orientation. This repeatability simplifies the comparison of data from different experiments where changes in chromium doping or structure are being studied.

For the $\theta = 54.7^{\circ}$ orientation, emission was successfully obtained, using crystals of five different chromium concentrations, for signal frequencies from 23.5 to 27 kMc, pump frequencies from 64.0 to 72.6 kMc, and magnetic fields from 10.3 to 12 kilogauss (Figure 9).

In accordance with theory, both the electronic gain and the inversion ratio were significantly higher in the high-field region than was obtained in the low-field region. Increased absorption and emission were obtained as the chromium concentration was increased from 0.10 percent starting Cr_2O_3 to 0.40 percent starting Cr_2O_3 (Figure 9). The crystal with 0.40 percent starting Cr_2O_3 gave inferior results, indicating that an optimum chromium concentration appears to exist. In

each case, the active crystal was 1/2 inch in length. Table II lists the starting and the final chromium concentrations of the crystals tested.

The best data were obtained using the rutile crystal with 0.25 percent starting Cr_2O_3. For the 54.7° crystal, the magnetic absorptions varied from 1.7 to 2.8 db, and the electronic gain varied from 3.5 to 5.7 db (Figure 9A) at 4.2° and averaged 4.4 db (8.8 db per inch). The measured inversion ratios are shown in Figure 9B . These are conservative absorption and gain measurements, since gains up to 8 db have been measured. The variations in the curves are due to internal mismatches that cause regeneration at certain frequencies. This problem is eliminated when isolators are incorporated into the structure.

When the liquid helium bath temperature was reduced from 4.2°K to 1.6°K, the absorption increased by a factor of 1.75 and is in reasonable agreement with the calculated value of 1.60. The average electronic gain in the 23 to 27 kMc band increases from 8.8 to 21 db per inch at 1.6°K.

Emission was next obtained from 33.5 to 39.5 kMc, with a chromium-doped rutile crystal oriented at $\theta = 80°$, $\phi = 25.7°$, using a pump frequency from 62 to 76 kMc and magnetic fields from 8.5 to 12 kilogauss.

The average magnetic absorption for the 80° crystal was 5.0 db per inch, and the electronic gain averaged 5.4 db per inch at 4.2°K. When the temperature was reduced to 1.7°K, the absorption increased to 8.4 db per inch, and electronic gain was 14 db per inch. The chromium concentration was not optimum in the crystal tested, and for an optimum concentration the measured electronic gain of 14 db per inch can be expected to increase to 17 db per inch.

TABLE II

STARTING AND FINAL CHROMIUM CONCENTRATIONS FOR TiO_2 CRYSTALS

Starting Concentration		Final Concentration	Ratio of Final to Starting Concentration
Percent of Cr_2O_3 by weight	Percent of Cr^{+3} by weight	Percent of Cr^{+3} by weight	
0.15	0.102	0.016	0.16
0.10	0.069	0.025	0.36
0.20	0.136	0.054	0.40
0.25	0.171	0.065	0.38
0.30	0.205	0.075	0.37
0.40	0.272	0.093	0.34

C. EXPERIMENTAL AND CALCULATED STRUCTURE LOSS

Although our matching sections were not optimized, an average input SWR of 1.65 and an average structure loss of 5 db (including input and output waveguide runs) were measured from 23 to 30 kMc at $4.2^{\circ}K$ in a copper structure loaded with a half-inch piece of rutile.

As the length of the active crystal is increased, the electronic gain and the losses in the active section (in decibels) increase in direct proportion to the length of the crystal, but the losses in the input and output waveguide, the U-turn, and the input and output waveguide sections remain constant.

On the basis of the measured data, it is estimated that the structure loss of a copper structure with 2-1/2 inches of active material would be 10.5 db at $4.2^{\circ}K$.

D. PUMP SATURATION

A representative curve of electronic gain as a function of pump power attenuator setting is shown in Figure 10. The curve shows that the 1/2-inch long high-concentration crystal is inverted with an attenuator setting of 21 db, which corresponds to an estimated incident pump power level of 0.3 mw. With the pump attenuator at 0 db (estimated to be 30 mw from the pump source), the slope of the electronic gain appears flat, indicating saturation.

E. LINEWIDTH

A prime cause for the relatively low magnetic absorptions and emissions appears to be the unusually large linewidth of the magnetic resonance. Table III summarizes the measurements. These measured linewidths are substantially larger than the 7 to 35 gauss linewidths reported by Sabisky

TABLE III

SUMMARY OF LINEWIDTH MEASUREMENTS

Transition	Concentration in Percent Chromium	Orientation (degrees) θ	Orientation (degrees) ø	Number of Sites	Magnetic Field Region	Linewidth (gauss)
Signal	0.075	54.7	45	2	Low	62
Signal	0.065	54.7	45	2	High	92
Signal	0.065	60.0	40	1	High	100
Signal	0.065	62.5	-	1	High	135
Idler (push-pull orientation)	0.054	54.7	45	2	-	50

and Gerritsen (references 6 and 7) and by Geusic (reference 8). The large linewidths may be due to:

1. Inhomogeneous Magnetic Field.--Magnetic absorptions and linewidths, measured in the AIL 4-inch magnet, were compared with measurements that we made in a 12-inch magnet at Polytechnic Institute of Brooklyn. The measurements were in good agreement, leading to the conclusion that the magnetic field of the AIL 4-inch magnet is sufficiently homogeneous over the 1/2-inch maser crystal.

2. Variation of Crystalline Electric Field Parameters D and E through Maser Crystal.--This possibility would broaden the signal transition more than the idler transition. This has been observed by us (see Table III) and is confirmed by data from Sabisky and Gerritsen who measured 35 gauss for a transition involving the zero-field splitting, but 7 to 21 gauss for transitions not involving the zero-field splitting. However, the effect of D and E decreases as the magnetic field is increased, so that narrower linewidths would be expected at high fields. This has not been observed.

3. Variation of Crystal Angular Orientation.--This might be caused by warpage of the structure, unparallelism of the crystal or structure surfaces or uneven pressure on the crystal (since pressure on the crystal could cause a shift in resonant frequency). Variation of the crystalline c- and/or a-axes could cause a similar effect.

   In the high magnetic field region, θ and ϕ take on a more predominant effect on the energy level distribution. The slopes $\partial f/\partial\phi$ and $\partial f/\partial\theta$ vary with the angular orientation of the crystal and show the effect of any slight unparallelism of the crystal with respect to the magnetic field. At the $\theta = 54.7^\circ$, $\phi = 45^\circ$ orientation, the parameter $\partial f/\partial\phi$ is about 350 Mc/degree, and $\partial f/\partial\theta$ is about 100 Mc/degree. A variation of ϕ of only $1/4^\circ$ would broaden the maser resonance line from 20 to 90 Mc.

   The $54.7/45^\circ$ orientation is particularly susceptible to this type of broadening because, in the Spin Hamiltonian (reference 6), ϕ occurs in the form $\cos 2\phi$, which has its maximum variation in the region of $\phi = 45^\circ$. Any slight unparallelism is therefore reflected in a substantial line broadening.

VI. FERRITE ISOLATORS

To achieve stable operation in the presence of internal structure mismatches and load mismatches, ferrite isolators were incorporated into the maser structure. To ensure unconditional stability, the reverse loss due to the isolators must be larger than the gain for one traversal of the signal forward and backward through the structure.

It is known from theoretical (reference 4) and experimental work (reference 9) that when a dielectric slab is mounted in a coaxial line or waveguide, regions of nearly pure circular polarization are achieved at the air-dielectric interface. Accordingly, a neat way of designing a ferrite-loaded rutile maser would be to use disks or slabs against the side of the active rutile sliver.

A 0.200 × 0.020 × 0.0005-inch slab of nickel-zinc ferrite was incorporated into the maser structure. Good nonreciprocity was obtained to demonstrate the feasibility of this technique. Figure 11 shows the results of room temperature measurements of the reverse loss of the 0.200-inch-long piece of ferrite versus the applied magnetic field with signal frequency as a parameter.

The ferrite linewidth was measured to be 900 gauss at room temperature. At $4.2^{\circ}K$, the ferrite linewidth increased to more than 1500 gauss, and the ferrite tuning curve overlapped the rutile tuning curve ($\theta = 80^{\circ}$) from 33 to 41 kMc. The ferrite slab contributed a forward loss of less than 0.5 db and an average reverse loss from 25 to 40 db, thereby ensuring stability of the maser amplifier.

These ferrite slabs were incorporated into a maser structure and proved successful in suppressing oscillations due to structure mismatches.

VII. FINAL PACKAGING CONSIDERATIONS

A. FINAL MASER PACKAGING CONSIDERATIONS

Based on the experimental results of the present phase, an estimate was made of the final maser amplifier package that could operate over the 27 to 40 kMc band.

1. STRUCTURE

Based on the measured electronic gains of 14 db per inch at $\theta = 80^{\circ}$, $\phi = 25.7^{\circ}$ at $1.7^{\circ}K$, it is estimated that 25 db of net gain can be achieved in a physical length of only 2-1/2 inches by folding the structure in half to reduce the overall length of the package. The physical dimensions of the active section for the final model determine the size, shape, and weight of the helium dewar and magnet. A full-length structure (Figure 12), loaded with active material on both input and output to reduce physical length and magnet requirements, has been fabricated and tested. As can be seen, the waveguide turn at the bottom of the structure is made in reduced-height waveguide.

The input SWR of the structure averaged 1.8, and the insertion loss averaged 14.5 db at liquid nitrogen temperatures when tested from 27 to 39 kMc. These losses would be reduced to about 10.5 db when the structure is cooled to liquid helium temperatures. The structure was made of red brass, and by copper-plating further reductions in insertion loss will be obtained. The structure was fabricated so that the pump signal can be brought down its own transmission line and introduced into the signal line at the waveguide turn. This technique takes advantage of all the available pump power, rather than sacrificing 3 db, as is done presently by introducing the pump through a waveguide tee on the input.

2. HELIUM DEWAR

It is estimated that the full-length structure can be mounted in a metal dewar flask, whose tail would have the following geometry to minimize magnet weight.

The tail could be either rectangular or race-track shaped with the magnetic field vector through the narrow dimension, which could measure 0.800 inch O.D. × 0.480 inch I.D. in order to accommodate the full-length structure, which is 0.350-inch thick. The wide dimension of the dewar tail should be a minimum of 1.10 inches I.D. to accommodate the width of the maser structure and a pump input waveguide that would feed the maser structure from the bottom by means of a tee, giving an equal power split between the two halves. Measurements have shown that the discontinuity of the RG-99/U (60 to 90 kMc) waveguide narrowed down to 0.030 × 0.122 inch introduced only a small mismatch into the signal waveguide.

3. MAGNET

A 4-inch-diameter electromagnet, capable of supplying 16 kilogauss across a 0.850-inch gap, has been designed for this maser by Dr. H. Roters, magnet consultant. This advanced design incorporates various weight-saving features such as the use of cobalt-iron alloy. The estimated weight of the magnet is 215 pounds, and its power dissipation is 1580 watts for a temperature rise to 90°C.

A superconducting magnet using either the recently discovered niobium-three-tin or niobium-zirconium superconducting wire is estimated to weigh less than 5 pounds and to fit in a cylinder 5 inches in diameter and 5 inches high. Further work on this magnet is in progress.

4. PUMP SOURCE

At present, tunable klystrons delivering 100 milliwatts are available. For fast tuning, a BWO would be required. A 4-millimeter BWO of the required power level is not available at present, but it is within the state of the art.

B. FURTHER IMPROVEMENTS

1. RESONANT SLOWING

Data has been presented on a TWM that has large tuning ranges and high gains. It uses a small volume of active material by taking advantage of the inherent slowing of rutile (caused by its high dielectric constant). Resonant slowing techniques can also be used, so that higher gains per unit length can be achieved. Figure 13 shows a calculated curve of insertion loss and slowing factor versus signal frequency for a novel periodically ridged corrugated waveguide filter structure. As can be seen, an average slowing of 2.6 can be realized over a 25-percent tuning range. Since the high-frequency band can be covered by two maser structures, each with tuning ranges of less than 25 percent, resonant. slowing could be used without degrading the proposed tuning range.

This type of structure has alternate stop and pass bands. Figure 13 shows the pump tuning range to be in a pass band; thus, this additional signal frequency slowing does not require any additional pump power.

2. EFFECT OF REDUCED LINEWIDTH

High field signal linewidths of 92 to 100 gauss are reported in Section V, paragraph E of this report. Since the electronic gain varies inversely with the linewidth, a substantial increase in electronic gain per unit length would be expected if the linewidth were reduced to its reported value

of 7 gauss. The different possible causes of line broadening mentioned are still being investigated.

It should also be noted that, though a broadened resonance line decreased our electronic gain, it also has the effect of increasing our instantaneous bandwidth.

3. OPTIMUM DOPING

The heavily doped boule of titania that gave poor absorptions and inversions is being studied to see if the chromium went into the trivalent state. Since the material is relatively new, and the growing techniques have not been fully refined, there is a possibility that the chromium does not go into the correct valence state when the concentration is so high.

Any data on optimum doping must be considered tentative until further investigations are made.

VIII. CONCLUSIONS

The feasibility and design for a new K_a-band maser have been successfully tested. This maser is of the traveling-wave type and features unprecedented tuning range, low noise factor, stability by use of ferrite isolators, and relatively low ($\approx$70 kMc) pump frequency. The design is applicable to signal frequencies from 12 to 150 kMc.

IX. REFERENCES

1. H. J. Gerritsen, S. E. Harrison, and H. R. Lewis, "Chromium-Doped Titania as a Maser Material," Journal of Applied Physics, Vol 3, p 1566-1571, September 1960.
2. D. P. Devor, "Fine Structure Levels and Transition Probabilities of Cr^{+3} in TiO_2 (Rutile)," Hughes Research Report 148, May 1960.
3. H. J. Gerritsen, First Quarterly Progress Report, Contract DA-36-039-sc-87386, Radio Corporation of America, 29 December 1960.
4. P. H. Vartanian, W. P. Ayres, and A. L. Helgesson, "Propagation in Dielectric Slab Loaded Rectangular Waveguide," IRE Trans, Vol MTT-6, p 215-222, April 1958.
5. "Electron Devices Research," Stanford Electronics Laboratories Consolidate Quarterly Status Report, No. 8, p 18, 1 October to 31 December 1958.
6. H. J. Gerritsen, S. E. Harrison, H. R. Lewis, and J. P. Wittle, "Fine Structure, Hyperfine Structure, and Relaxation Times of Cr^{+3} in TiO_2 (Rutile)," Phys. Rev. Letters, Vol 2, p 153-155, 1959.
7. E. S. Sabisky, H. J. Gerritsen, "A Traveling-Wave Maser Using Chromium-Doped Rutile," Proc IRE, Vol 49, p 1329-1330, August 1961.
8. J. E. Geusic, First Quarterly Report, Contract DA-36-039-sc-85357, Bell Telephone Laboratories, 20 September 1960.
9. F. R. Arams, B. Kaplan, and B. Peyton, "Octave-Bandwidth UHF/L-Band Circulator," Presented at PGMTT Symposium, Washington, D. C., May 1961, IRE, Transactions MTT-9, p 212 - 216, May 1961.

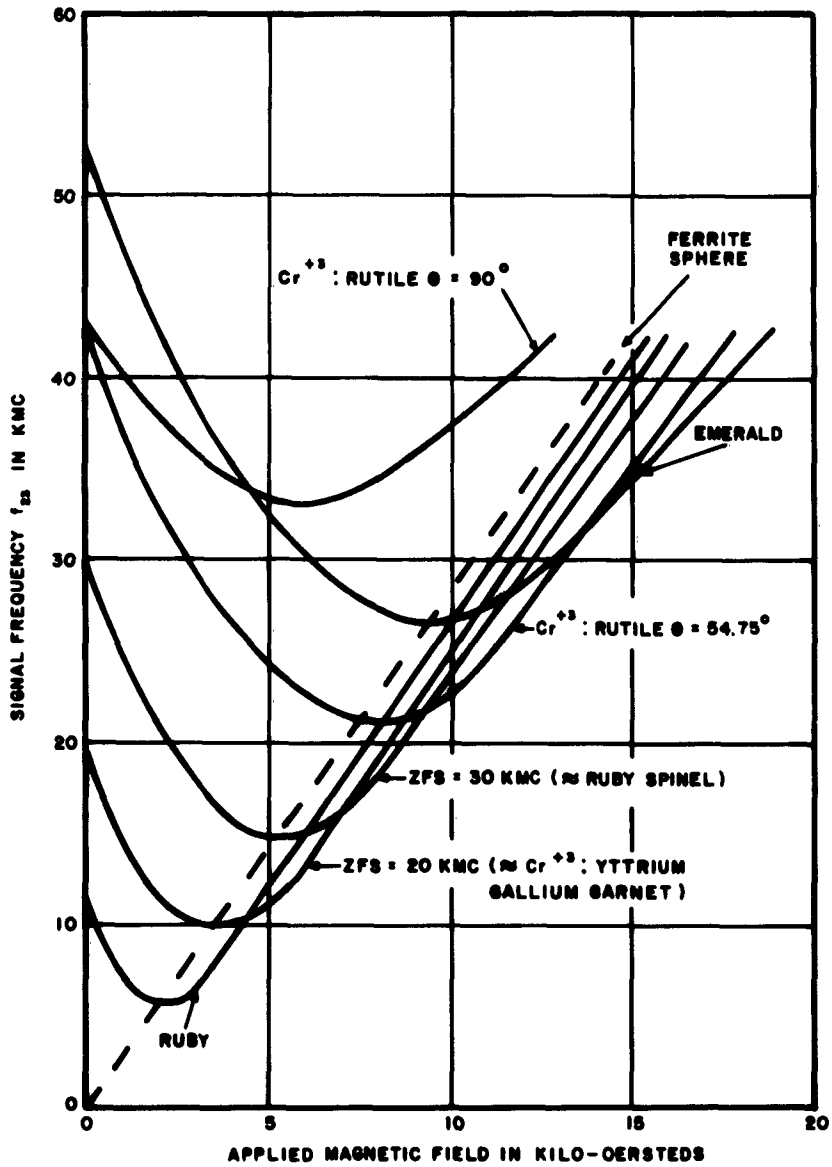

FIGURE 1. COMPARISON OF VARIOUS PUSH-PULL-PUMPED MASER MATERIALS

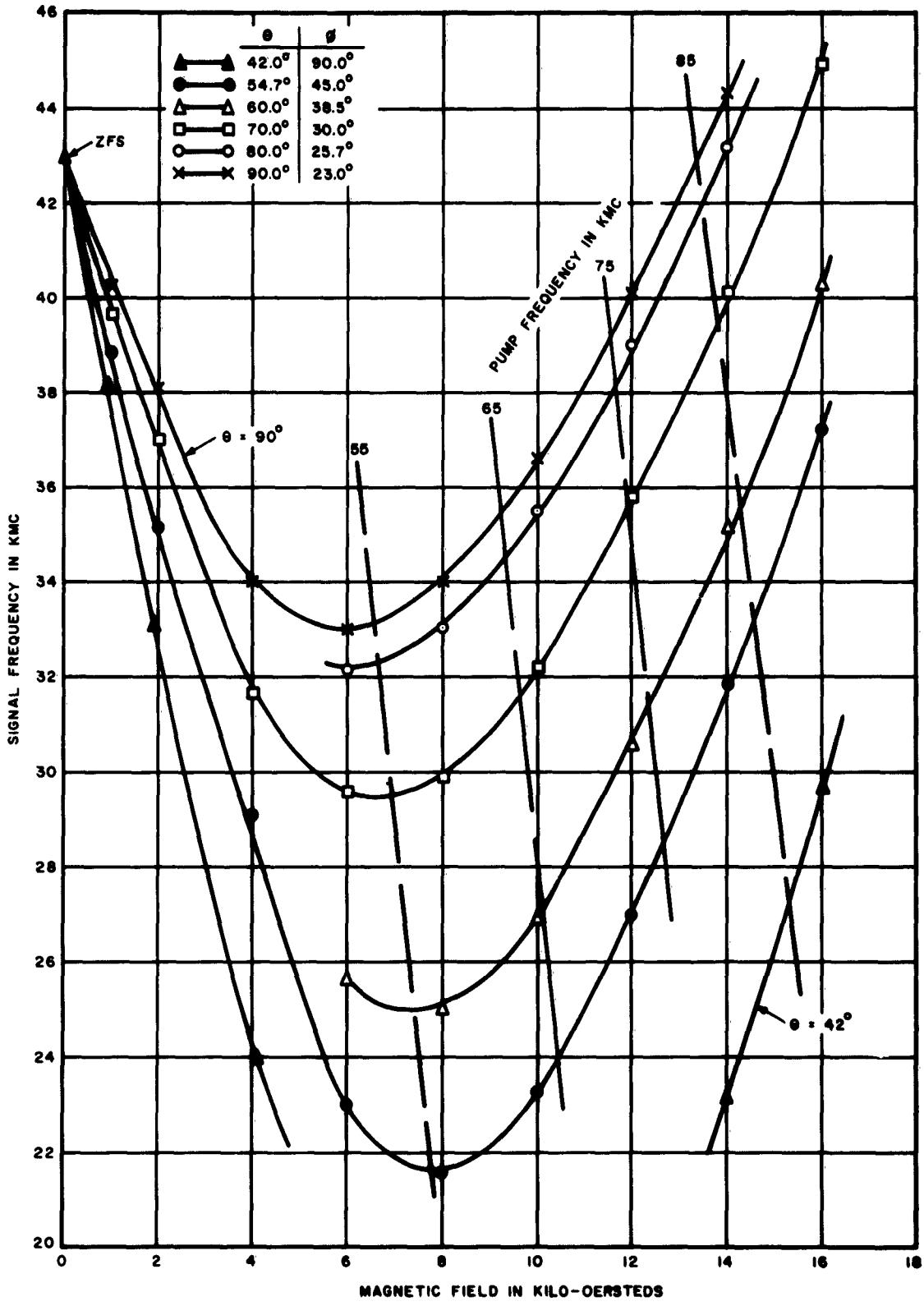

FIGURE 2. SIGNAL FREQUENCY VS MAGNETIC FIELD FOR PUSH-PULL-PUMPED CHROMIUM-DOPED RUTILE

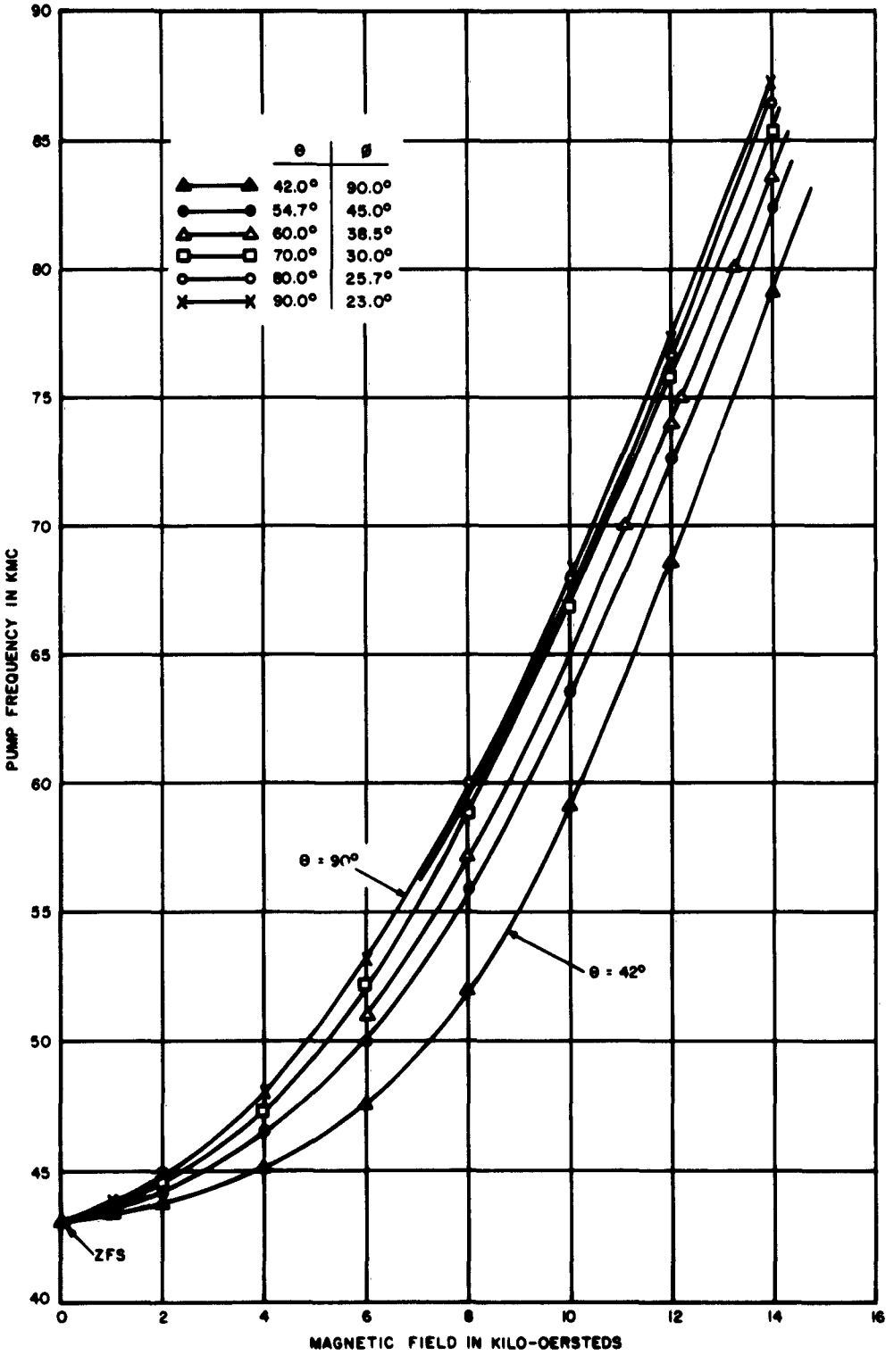

FIGURE 3. PUMP FREQUENCY VS MAGNETIC FIELD FOR PUSH-PULL-PUMPED CHROMIUM-DOPED RUTILE

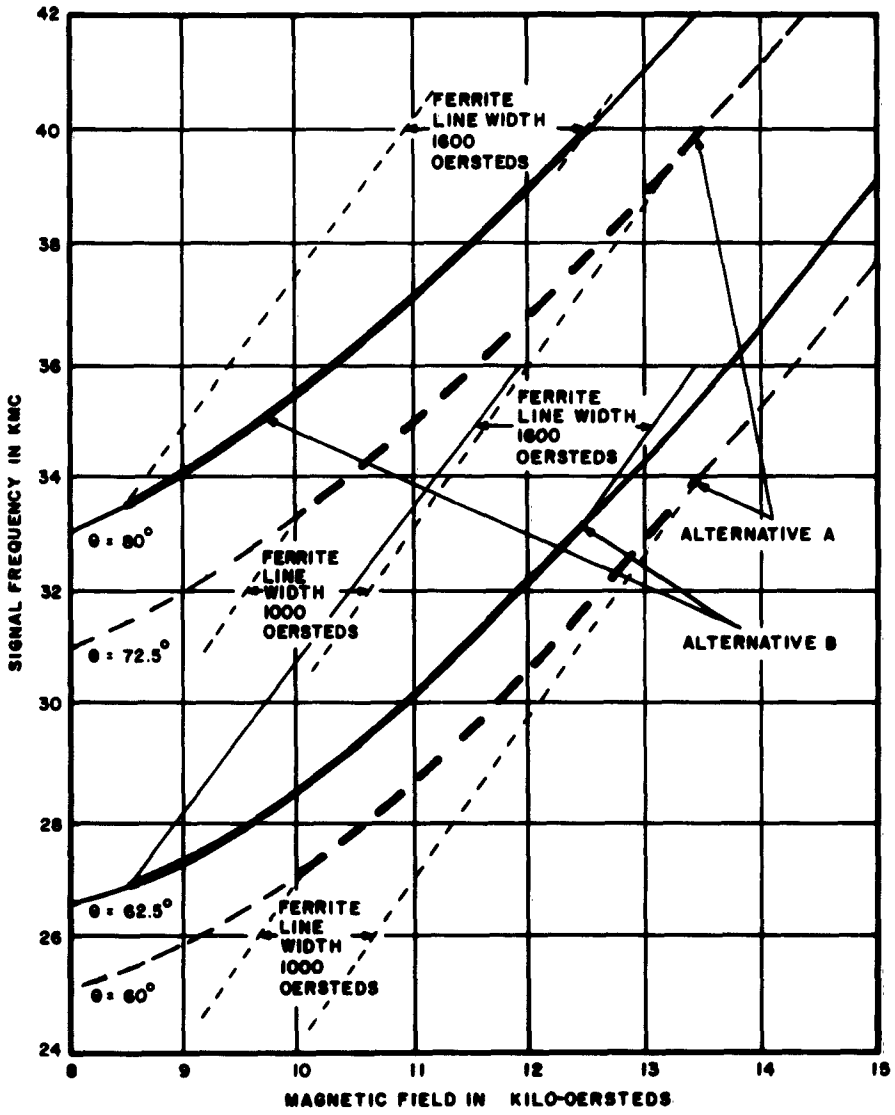

FIGURE 4. CALCULATED RUTILE TUNING CURVES

FIGURE 5. EXPERIMENTAL RIDGED WAVEGUIDE STRUCTURE LOADED WITH Cr^{+3} : TiO_2 CRYSTAL AND TWO POLYCRYSTALLINE MATCHING PIECES

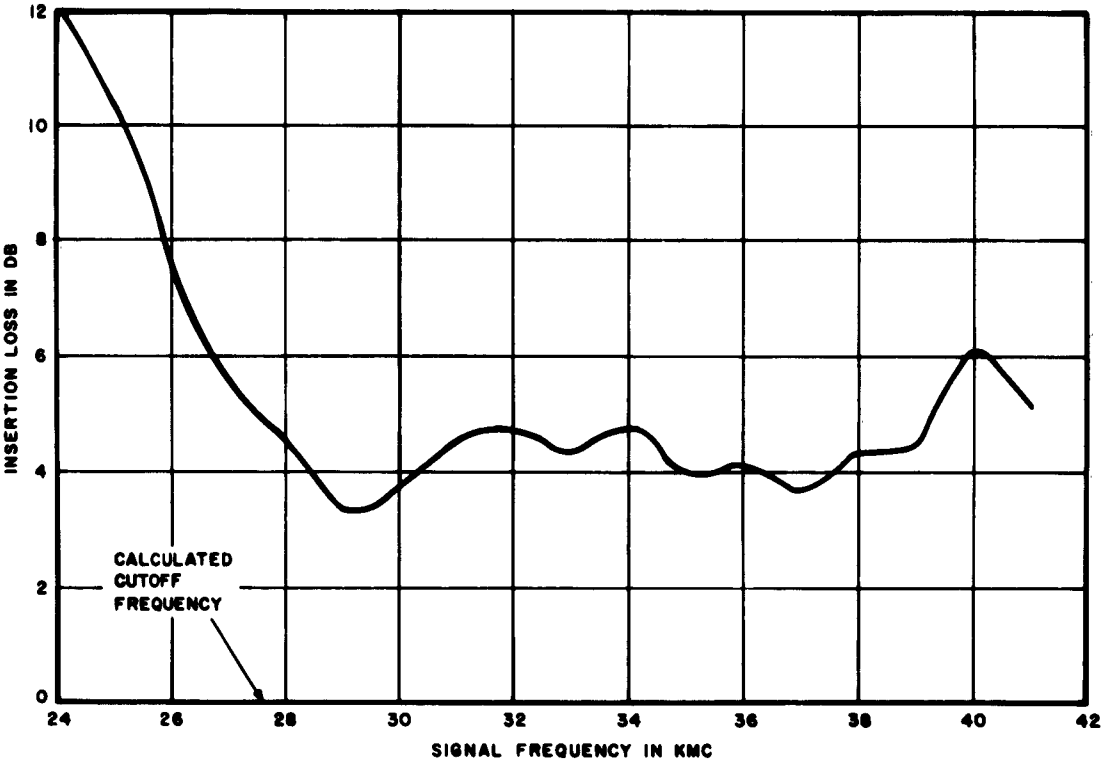

FIGURE 6. INSERTION LOSS OF TWM STRUCTURE AT ROOM TEMPERATURE

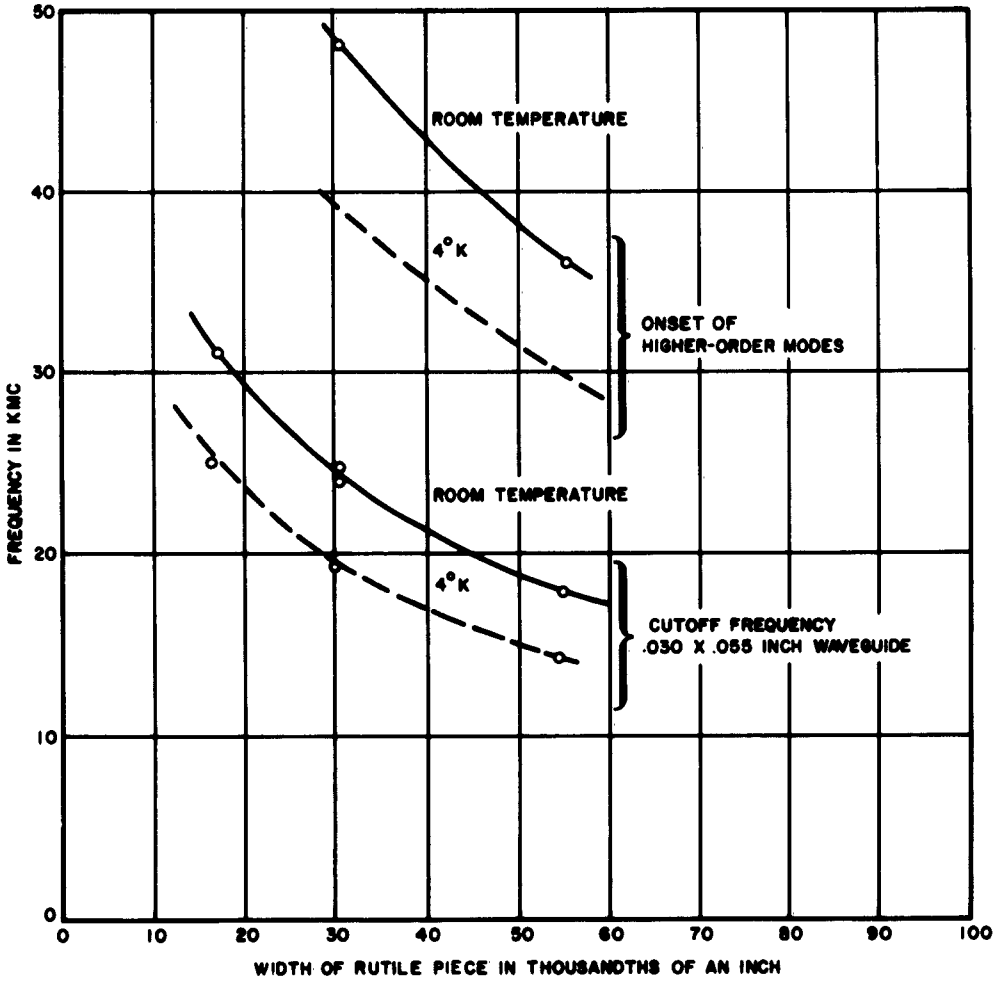

FIGURE 7. OPERATING FREQUENCIES FOR RUTILE-LOADED MASER STRUCTURE

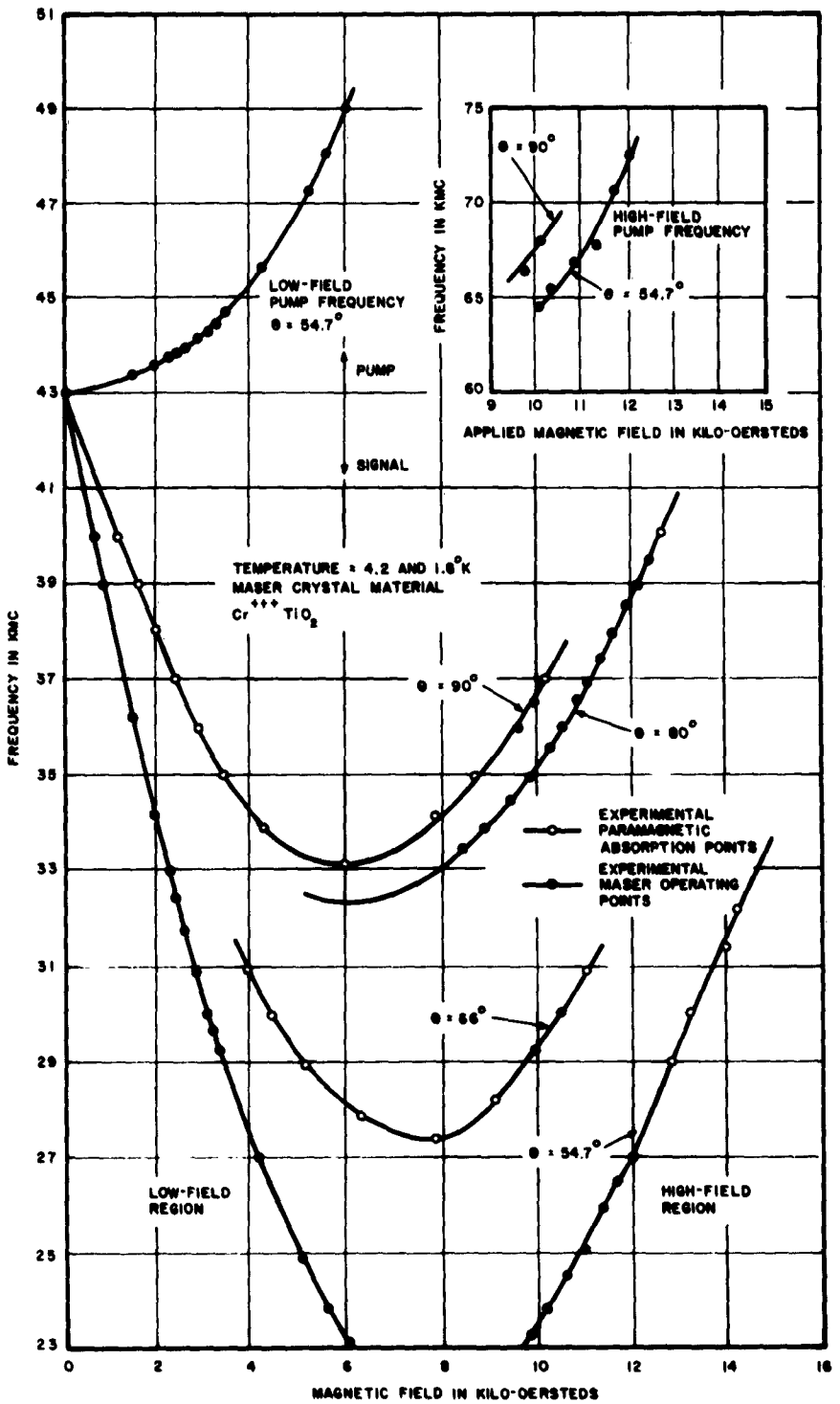

FIGURE 8. EXPERIMENTAL MASER DATA

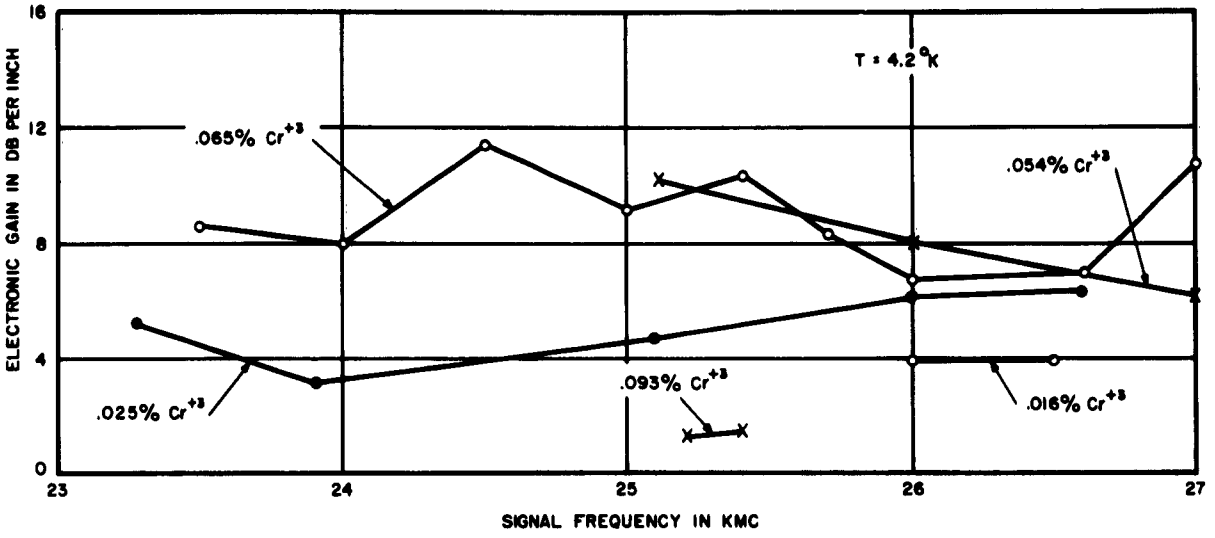

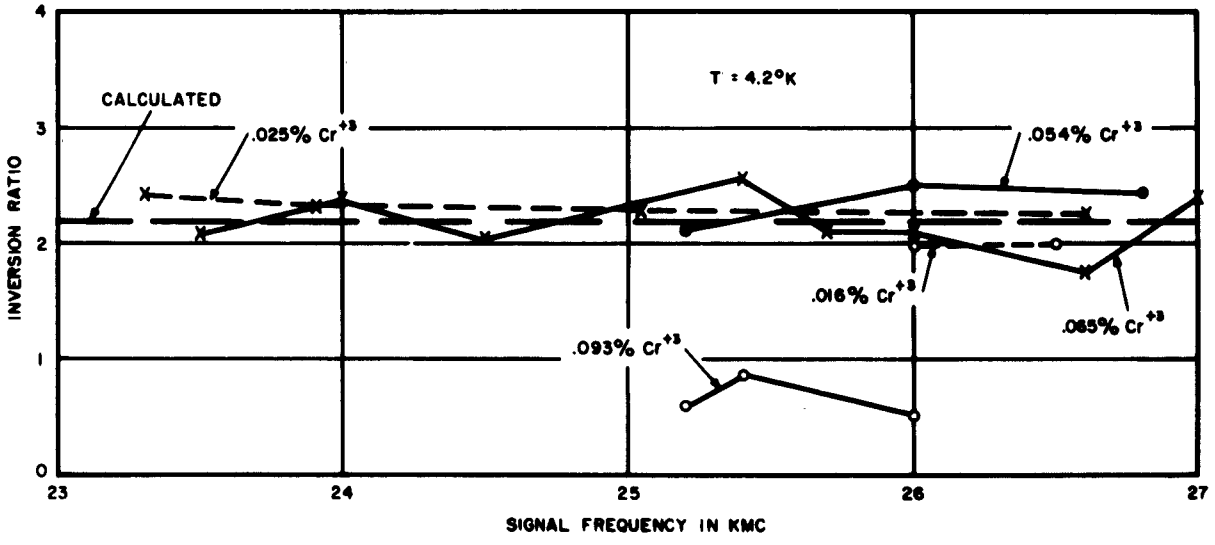

FIGURE 9. ELECTRONIC GAIN AND INVERSION RATIO VS SIGNAL FREQUENCY

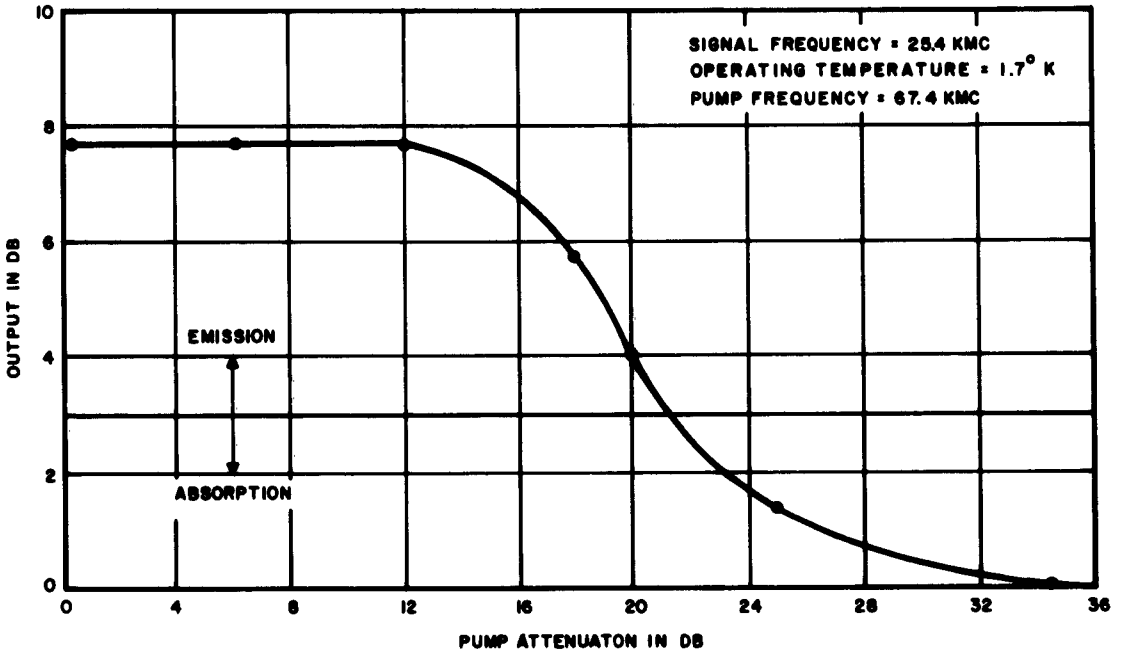

FIGURE 10. MASER PUMP SATURATION CURVE

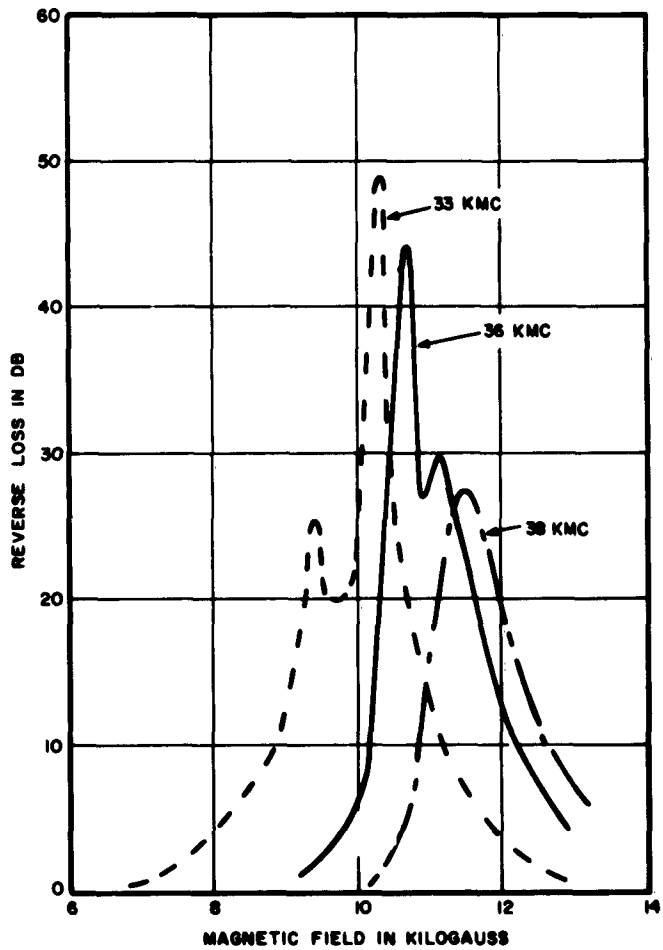

FIGURE 11. REVERSE ISOLATOR LOSS VS APPLIED MAGNETIC FIELD AT ROOM TEMPERATURE

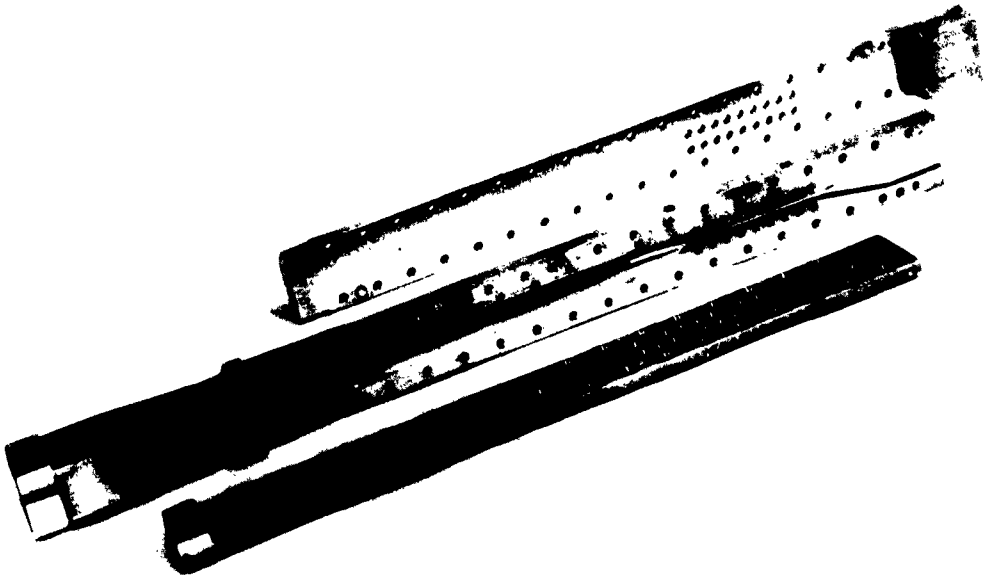

FIGURE 12. FOLDED TWM STRUCTURE HAVING AN ACTIVE LENGTH OF 2.3 INCHES

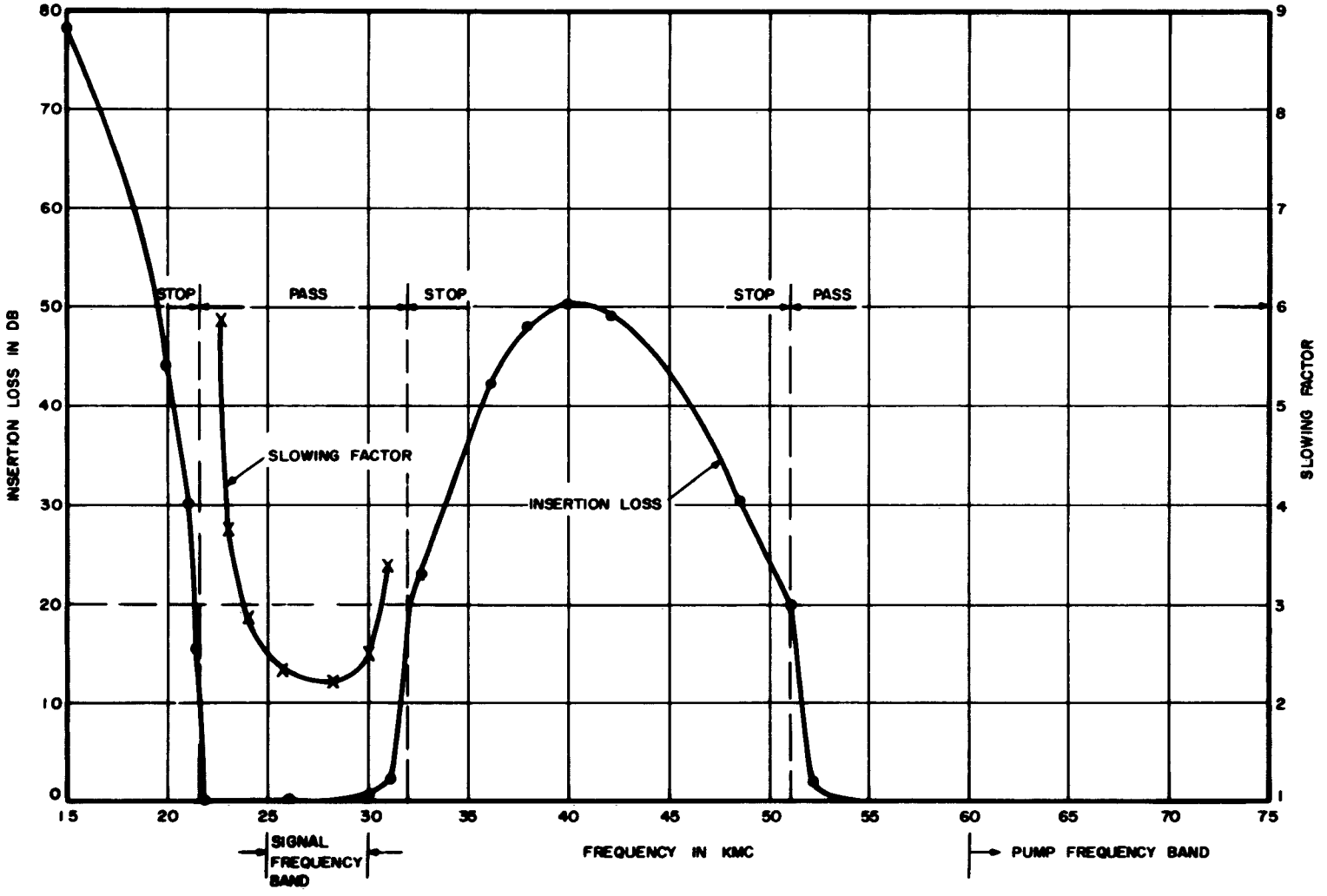

FIGURE 13. SLOWING FACTOR AND INSERTION LOSS VS FREQUENCY FOR RIDGED SLOW-WAVE STRUCTURE

APPENDIX

CALCULATED PERFORMANCE OF MILLIMETER-WAVE MASER USING PUSH-PULL PUMPING IN RUTILE

Calculations have been carried out without using the usual assumption, valid for microwave masers, that $hf \ll KT$. The calculations gave the following results:

THERMAL EQUILIBRIUM POPULATION DIFFERENCE

We obtain for the signal-frequency f_{23} transition

$$\frac{\eta_2 - \eta_3}{N} = \frac{1}{1 + \epsilon^{Af_{12}} + \epsilon^{-Af_{23}} + \epsilon^{-Af_{24}}} - \frac{1}{1 + \epsilon^{-Af_{34}} + \epsilon^{Af_{23}} + \epsilon^{Af_{13}}} \quad (1)$$

where $A = h/KT$.

The magnetic absorption obtained in a TWM is proportional to $\eta_2 - \eta_3$. In Figure A-1, the magnetic absorption at 30 kMc, normalized to the total spin population N, has been plotted as a function of idler frequency f_1, with bath temperature as a parameter. We see that for low-field operation ($f_1 \approx 10$ kMc), an increase in absorption approximately inversely proportional to temperature is obtained. However, for high-field operation ($f_1 \approx 40$ kMc), the absorption stays approximately constant (very unlike microwave maser behavior). This behavior can be explained by noting that, as the temperature is decreased, more spins go to level 1, so that fewer spins are available in levels 2 and 3 to give magnetic absorption.

PUMP-ON POPULATION DIFFERENCE

We obtain for the inverted population difference in the signal transition f_{23}:

$$\frac{\eta_3 - \eta_2}{N} = \frac{2\left(\epsilon^{Af_{12}} - 1\right) - \epsilon^{Af_{23}} + \epsilon^{A_{f_{14}}}}{2\left(4 + 2\epsilon^{Af_{12}} + \epsilon^{Af_{23}} + \epsilon^{Af_{14}}\right)} \qquad (2)$$

where $A = h/KT$.

The gain in db in a TWM is proportional to $\eta_3 - \eta_2$. Figure A-2 shows that, even for our case when $hf \approx KT$, a significant improvement in gain is obtained when the bath temperature is decreased.

Figure A-3 shows the population inversion ratio to be expected in a millimeter-wave push-pull maser.

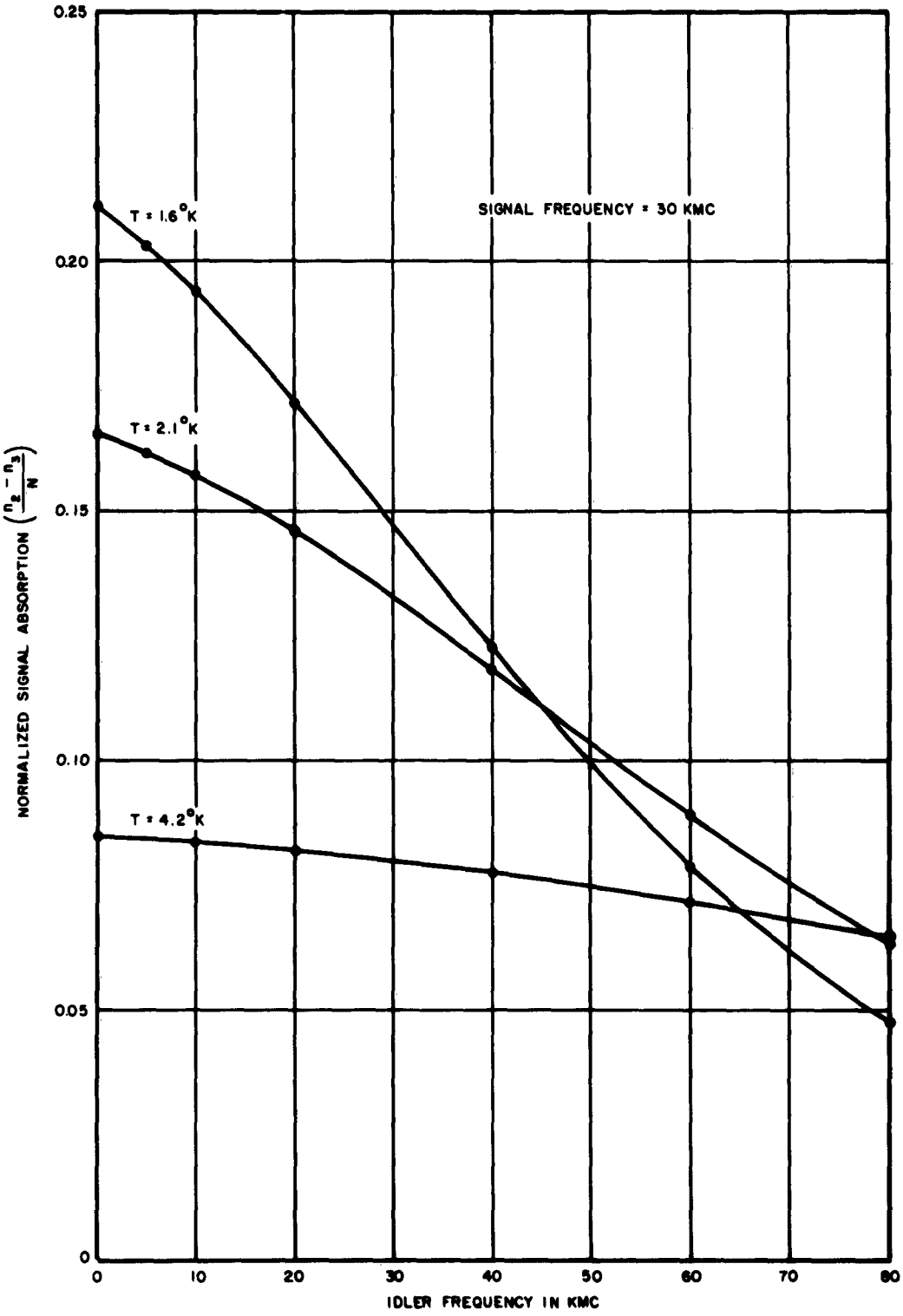

FIGURE A-1. NORMALIZED SIGNAL ABSORPTION VS IDLER FREQUENCY WITH BATH TEMPERATURE AS A PARAMETER

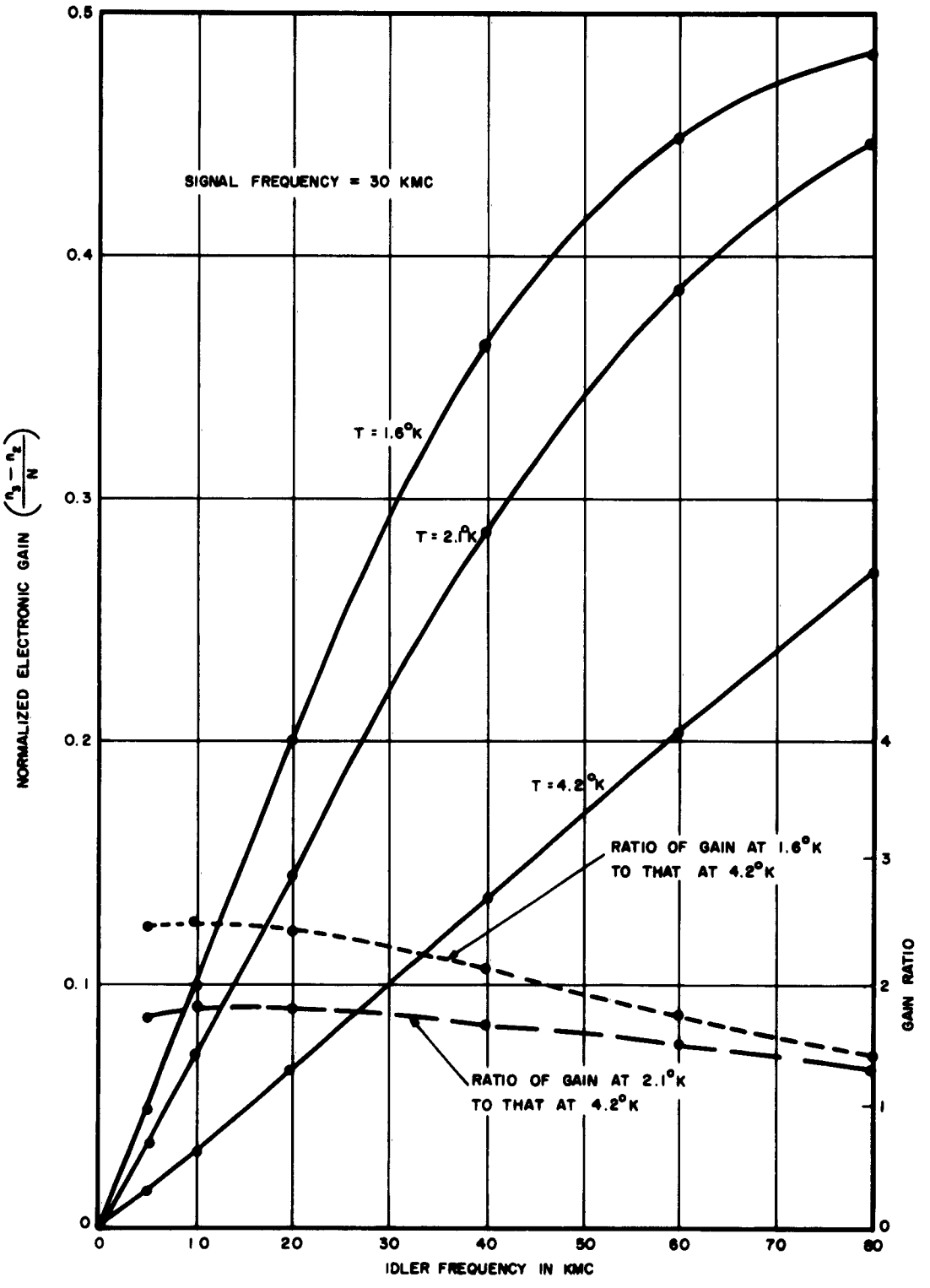

FIGURE A-2. NORMALIZED ELECTRONIC GAIN VS IDLER FREQUENCY WITH BATH TEMPERATURE AS A PARAMETER

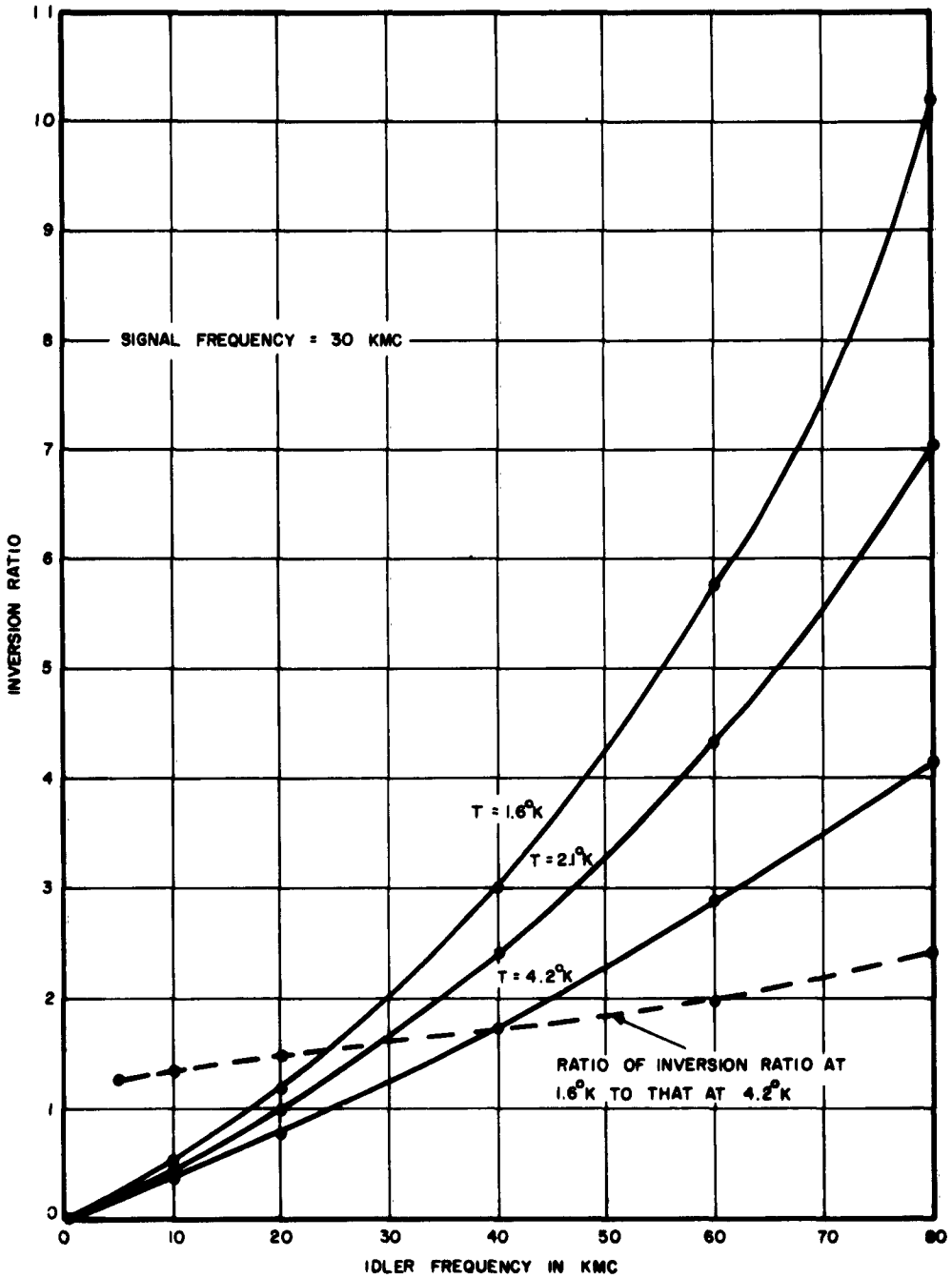

FIGURE A-3. CALCULATED INVERSION RATIO VS IDLER FREQUENCY WITH BATH TEMPERATURE AS A PARAMETER